Islamic Azad University

Journal of

Optoelectronical Nanostructures

Volume 10, Issue 1, Spring 2025, Page 1-19

Research Paper

The impact of the plasmon-exciton interaction on the optical characteristics of the hybrid system $NPVO_2 - QD - NPVO_2$

Abdolrasoul Gharaati*[,1], Ghasem Forozani[1], Esmail Salari Sardoi[1]

[1]Department of Physics, Payame Noor University, Tehran, Iran

Received: 2024.09.12
Revised: 2025.01.08
Accepted: 2025.01.10
Published: 2025.05.05

Use your device to scan and read the article online

Keywords:
Optical properties, Quantum dot, Hybrid system, Forster broadening, Exciton energy transfer

Abstract

In this paper, the optical characteristics of a plexitonic system comprising two $NPVO_2$ and one quantum dot (QD) were investigated. Both $NPVO_2$ and QD have unique optical properties on their own and their combination in the hybrid system $NPVO_2$-QD-$NPVO_2$ can lead to interesting phenomena. In this method, when the $NPVO_2$ and QD nanoparticles (NPs) and their resonance frequencies are close to each other, due to the interaction between $NPVO_2$ plasmons and QD excitons, the optical characteristics of QD change. In this paper, the changes in the optical properties of QD near $NPVO_2$, a crystalline material whose phase changes from semiconducting to metallic at a critical temperature, were investigated. Based on the results, the proximity of $NPVO_2$ to a QD caused an energy shift and an absorption peak which are also used in sensor applications. Moreover, the Förster broadening as well as exciton energy transfer were also investigated. It was revealed that they changed because of the interaction of the dipoles between the plasmons and excitons.

Citation: Abdolrasoul Gharaati, Ghasem Forozani, Esmail Salari Sardoi. The impact of the plasmon-exciton interaction on the optical characteristics of the hybrid system $NPVO_2$-QD-$NPVO_2$. **Journal of Optoelectronical Nanostructures.** 2025; 10 (1): 1-19

***Corresponding author:** Abdolrasoul Gharaati
Address: Department of Physics, Payame Noor University, Tehran, Iran.
Email: agharaati@pnu.ac.ir
DOI: https://doi.org/10.71577/jopn.2025.1210141

1. INTRODUCTION

Fundamental research in the field of nanophotonics primarily focuses on understanding the optical excitations induced by nanoscale materials and how the characteristics of these excitations depend on the size, shape, and arrangement of nanostructures. Two types of excitations that have garnered significant attention from researchers are plasmons in metallic nanostructures and excitons in molecular materials or semiconductors. Plasmons are the collective oscillations of free electrons in metals. The coupling of light with plasmon resonance has attracted considerable interest because it can concentrate light fields in volumes much smaller than the diffraction limit [1]. Excitons are bound pairs of electrons and holes in semiconductors or molecules and have gained considerable attention in quantum dots (QDs) or semiconductor nanocrystals due to their size-dependent frequency transitions and effective light emission [2-5].

Recent advancements in nanostructure fabrication techniques have enabled scientists to blend various nanoparticles (NPs) with contrasting optical characteristics into multi-structured nanocomposites, offering exciting possibilities to alter specific optical characteristics in the constituting NPs [1-8].

A substantial number of studies in this field have explored the interaction of excitonic systems in semiconductor QDs and plasmonic nanostructures, providing excellent opportunities for controlling the interaction of matter and light as well as the flow of electromagnetic energy [9-11].

Given that optical excitation occurs in the form of excitons and plasmons in quantum dots (QDs) and metal NPs, respectively, QDs and metal NPs are examined through quantum mechanics and classical mechanics, respectively. When an electric field is applied, the plasmons in the metal nanoparticle are excited, creating a field around the nanoparticle that enhances the local field nearby. This local field also excites the excitons in the QD, resulting in a coupling between the plasmon and exciton, which leads to various intriguing effects including energy transfer, exciton energy changes, and an increase in the local field [12]. Theoretical studies on the metal nanoparticle-semiconductor QD (MNP-SQD) system have predicted Förster energy transfer facilitated by plasmons [8], modifications to spontaneous emission in semiconductor QDs [14], third-and fifth-order optical processes of tunable exciton-plasmon hybrid nanosystem [15], increase in the induced fluorescence of QD [16], tunnelling induced transparency [17], plasmonic two-photon switching phenomena [18], and control over energy transfer pathways in hybrid systems [19]. Numerous experimental studies have also been conducted on these combined systems. For instance, Mertens et al. studied silicon QD-AgNPs and demonstrated the

increase of QD photoluminescence in them [20]. Pons et al. developed a system comprising a gold NP and a CdSe/ZnS QD [21]. Vasa et al. constructed a nano-hybrid nanocomposite comprising a GaAs quantum well on a gold substrate [22]. They detailed a significant shift and broadening of the excitonic resonance in the quantum well because of the strong plasmon-exciton coupling. Additionally, they observed an increase in broadband electromagnetic absorption in a silicon film [23].

In this system, the Hamiltonian of the entire system, featuring two metal NPs on either side of the QD, is first calculated. The electric field experienced by the QD consists of three components: one is the employed external field, while the others are internal fields induced by the polarizations on both sides of the QD. Subsequently, using density matrix theory, the density matrix elements and the QD polarization are computed. Following this, the optical characteristics of the QD are examined.

In the current study, the optical characteristics of the $NPVO_2$-QD-$NPVO_2$ plexitonic system are investigated. First, $NPVO_2$ is introduced. Next, by controlling the temperature while maintaining the same structure, the changes in the QD properties due to $NPVO_2$ can be observed.

2. THEORETICAL MODEL

VO_2 has garnered significant attention due to its reversibility and phase transition temperature (approximately 68 ℃) [24]. This structural phase involves a transition from the monoclinic phase (at low temperatures, where it acts as an insulator or weak semiconductor) to the tetragonal rutile phase (at high temperatures, where it behaves as a metallic material). Following the phase transition, the electrical conductivity changes by a factor of 3 to 5, and the optical properties undergo substantial alterations. Various optical, thermal, and electrical devices have been proposed based on the metal-to-insulator phase change of VO_2 [25, 26].

The phase change in VO_2 can be induced by various applied forces, including intense radiation, external electric fields, hydrostatic pressure, and tension [27, 28].

Until a few years ago, many studies concentrated on VO_2 thin film materials with a phase transition temperature of 68 ℃. Nowadays, advancements in nano-material production have led to the synthesis of VO_2-based NPs using various chemical and physical methods. Moreover, their critical temperature has been reduced to room temperature. The two contrasting phases of VO_2 and their

mixture could be modeled by employing a filling fraction dependent on temperature which is 0 for the semiconducting phase and 1 for the metallic phase [29]. At medium temperatures (in phase transitions), matter is a mixture of two phases which is modeled by utilizing the effective medium theory, specifically the Maxwell-Garnett theory, in order to derive the dielectric function ε_{VO_2} [28]:

$$\varepsilon_{VO_2} = \varepsilon_{semi} \frac{(\varepsilon_{met}(1+2f) - \varepsilon_{semi}(2f-2))}{(\varepsilon_{met}(1-f) + \varepsilon_{semi}(2+f))} \quad (1)$$

in which f is the filling factor controlling the phase transition in $NPVO_2$. Fig. 1 shows the temperature changes of f which is a Bessel function for the heating and cooling modes in the vicinity of the critical temperature.

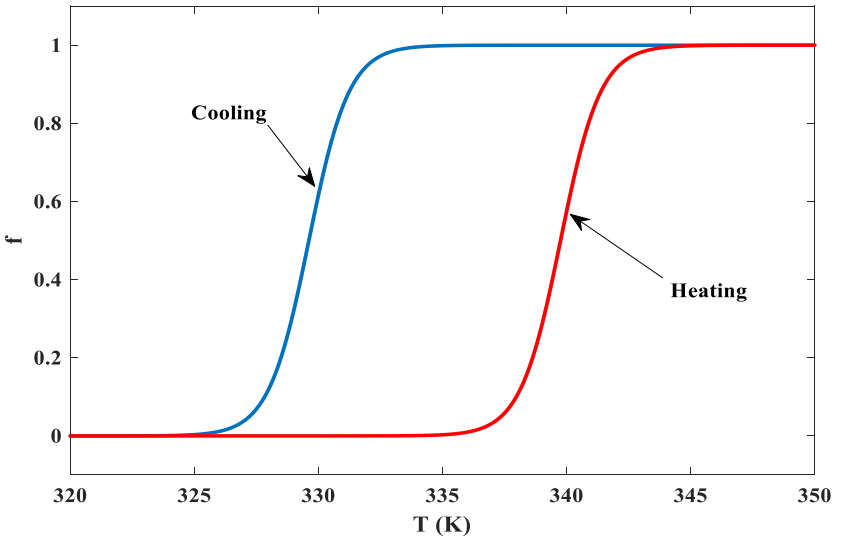

Fig. 1 The filling factor of VO_2 as a function of temperature [22]

ε_{semi} is the dielectric function of VO_2 in the semiconducting phase ($f = 0$), whereas ε_{met} is the dielectric functions of VO_2 in the metallic phase ($f = 1$) as shown below [28].

$$\varepsilon_{semi}(\omega) = 1 + \frac{(\varepsilon_n(i\infty) - 1)}{(1 - \omega^2/(\omega_\infty^2))} + \sum_{(i=1)}^{7} \frac{S_{n,i}}{1 - \frac{\omega^2}{\omega_{n,i}^2} - i\frac{\Gamma_{n,i}\omega}{\omega_{n,i}^2}} \quad (2)$$

$$\varepsilon_{met}(\omega)=1-\frac{\omega_{p,\tilde{n}}^2}{\omega(\omega+i\gamma_{\tilde{n}})}+\frac{\varepsilon_{\tilde{n}}(i\infty)-1}{1-\frac{\omega^2}{\omega_\infty^2}}+\sum_{i=1}^{4}\frac{S_{\tilde{n}.i}}{1-\frac{\omega^2}{\omega_{n,i}^2}-i\frac{\Gamma_{\tilde{n}.i}\omega}{\omega_{n,i}^2}} \quad (3)$$

where $\varepsilon_n(i\infty)=3.95$, $\omega_{p,\tilde{n}}=3.33eV$, $\gamma_{\tilde{n}}=0.66eV$, $\varepsilon_{\tilde{n}}(i\infty)=4.26$, and $\omega_\infty=15eV$. The other parameters in Eqn. (2) and Eqn. (3) are given in [26].

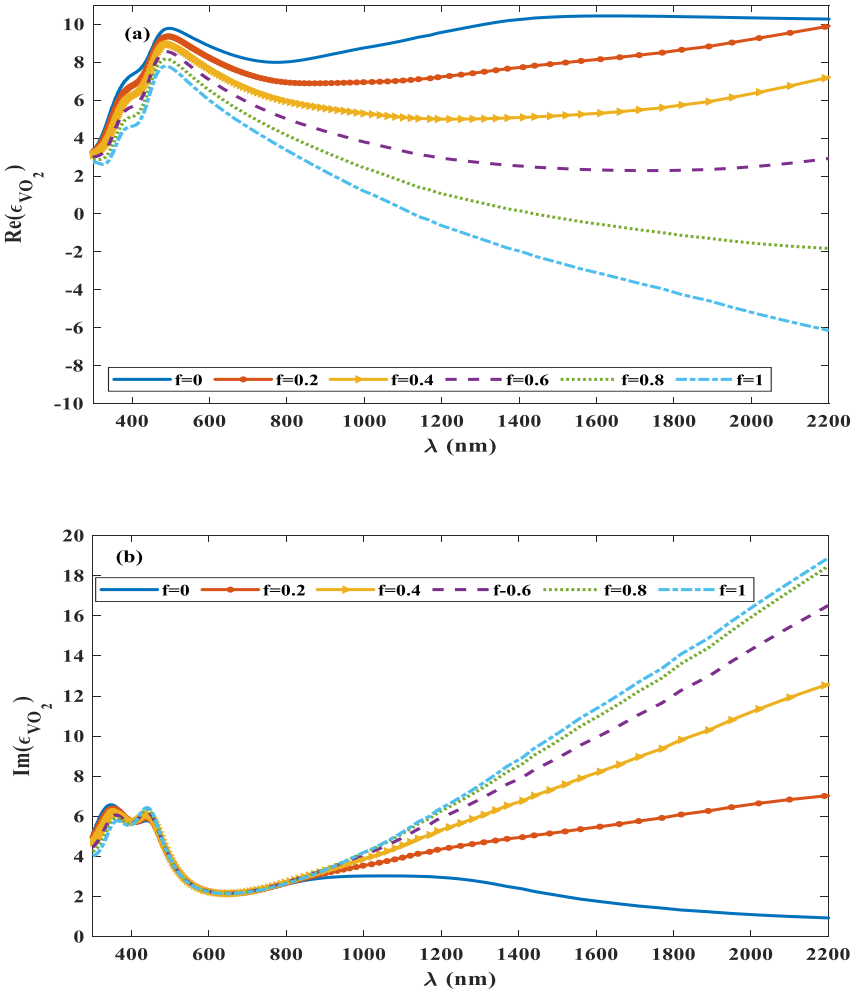

Fig. 2 a) The real and b) imaginary parts of the effective dielectric function ε_{VO_2} versus the incident wavelength for different filling fraction values

Fig. 2 illustrates the imaginary and real parts of the dielectric function versus the incident wavelength to show the dependence of the dielectric function ε_{VO_2} on the filling fraction. Fig. 2 (a) indicates that the real part of the dielectric function is negative for wavelengths above 1080 nm (energy = 1.14 eV). Consequently, at lower energies and higher filling fractions, VO_2 behaves similarly to a metal with a negative real part, leading to significant changes in the polarizability of $NPVO_2$ in the infrared region. These findings align well with previous studies on the optical characteristics of VO_2.

$NPVO_2$ is described by the multipole moment induced by an energy-dependent scalar polarizer. This polarizability could be managed by the ambient temperature which changes the filling fraction. The multipole polarizability could be given as [25]:

$$\beta_n = \frac{\varepsilon_{VO_2} - \varepsilon_b}{\varepsilon_{VO_2} + \frac{n+1}{n}\varepsilon_b} \quad (4)$$

where n stands for the multipole order so that the lowest order (n=1) represents the dipole order. ε_b is the dielectric function of the local background.

To demonstrate the dependence of the polarization of $NPVO_2$ on the filling fraction, using the finite element method for one $NPVO_2$ with a size of 40 nm, Fig. 3 (a) shows inside the silica material for different filling fraction values including metallic and semiconducting phases. Electromagnetic simulations were conducted using the finite-element method in COMSOL Multiphysics. The electromagnetic module was solved to obtain the distribution of the electric field, employing perfectly matched layers (PMLs) at a distance of half the maximum electromagnetic wavelength from the unit cell to prevent back reflection from the exterior boundaries. The PMLs around the unit cell minimize back reflection from the boundaries. These PMLs surround the unit cell, absorbing the excited mode from the source port and any higher-order modes generated by the periodic structure. In the metallic phase, the maximum absorption cross-section occurs at 1140 nm (energy=1.08 eV), whereas the maximum absorption cross-section in the semiconducting phase is at lower wavelengths. At this energy level, the amounts of absorption cross-section for metal and semiconductor are $\sigma_{abs} = 621\,nm^2$ and $\sigma_{abs} = 125\,nm^2$, respectively. According to the results, the transition from semiconductor to metal is enhanced about 5 times in the infrared region of the cross-section.

Figs. 3 (b) and 3 (c) illustrate the increase in the near-field at 1140 nm, shown as the amplitude of the scattered field relative to the incident field. The peak intensities for the metallic and semiconducting phases are respectively 2.2 and 1.5, indicating a symmetrical distribution. Notably, maximum absorption, based on the quasi-static approximation, occurs at 1140 nm, aligning with the resonance wavelength of surface plasmons in the metallic phase of $NPVO_2$.

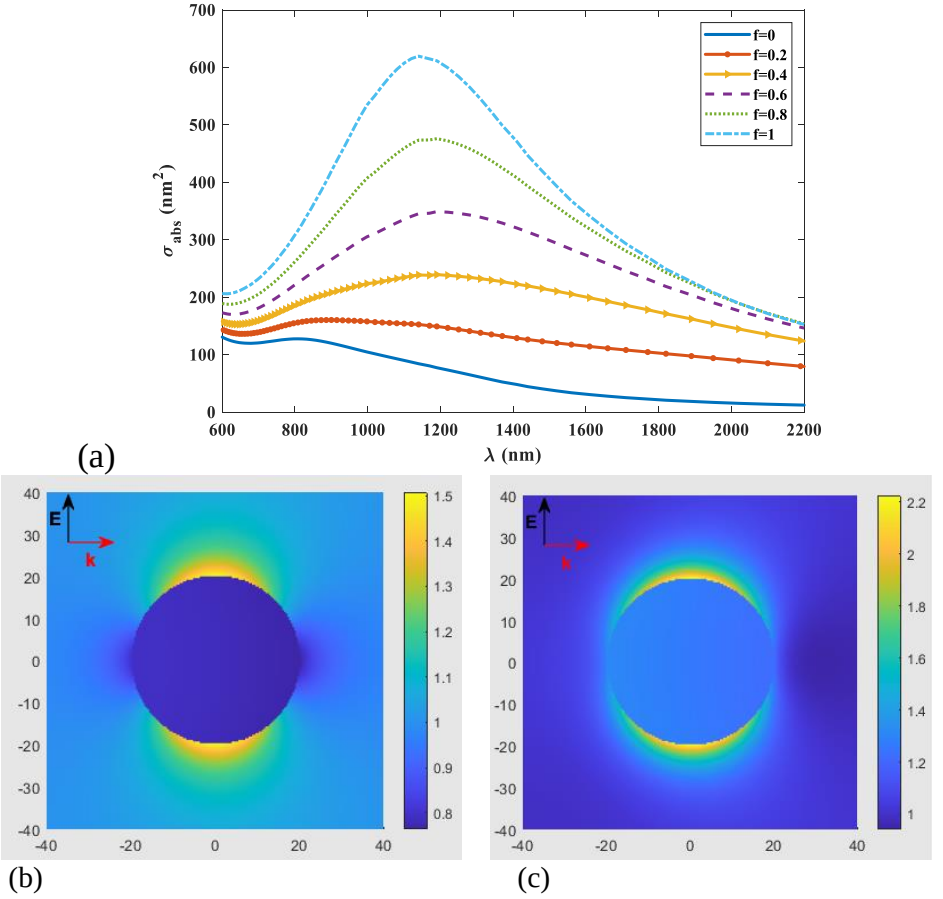

(a)

(b) (c)

Fig. 3 (a) Calculations of the finite elements of the absorption cross-section versus the wavelength for $NPVO_2$ in a silica medium. (b) and (c) Field enhancement at the wavelength of 1140 nm for the semiconducting and metallic phases, respectively

A. THE HYBRID $NPVO_2$-QD-$NPVO_2$ SYSTEM

In this section, the $NPVO_2$-QD-$NPVO_2$ hybrid system is discussed. QD optical excitations are classified as excitons, while nanoparticle excitations ($NPVO_2$) correspond to surface plasmon polaritons and surface polaritons in the metallic and semiconducting phases, respectively. When these NPs with distinct properties are placed adjacent to each other and subjected to an external field, the plasmons and excitons are excited, leading to Coulomb interactions between them. This dipole-dipole interaction becomes notably strong when the resonance frequencies of the NPs are closely aligned. The inclusion of metal NPs aims to enhance the interaction strength, while the plasmonic field generated nearby serves to improve both the linear and non-linear optical characteristics of the semiconductor QD.

Fig. 4 shows the QD (with radius a) between two $NPVO_2$ with radii R_1 and R_2. The center-by-center distance of the QD from the NPs is indicated by d_1 and d_2, respectively. The system is put in an environment with dielectric constant ε_b.

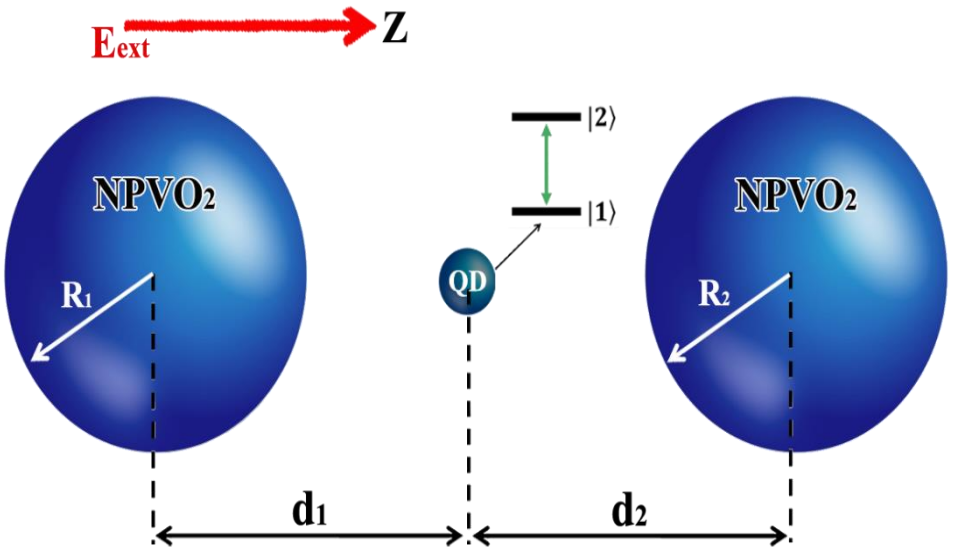

Fig. 4 The schematic of a $NPVO_2$-QD-$NPVO_2$ hybrid system with the $NPVO_2$ resonance frequency in the metallic phase which is close to the exciton transition frequency $|1\rangle \leftrightarrow |2\rangle$

B. The motion equations of the $NPVO_2$-QD-$NPVO_2$ system

According to Fig. 4, when the external electromagnetic field $E_{ext}(t) = E_0(e^{i\omega t} + e^{-i\omega t})$ is utilized for the system, the excitons and plasmons are excited in QD and $NPVO_2$, respectively. In addition, the QD senses two other induced fields owing to the polarization of $NPVO_2$. Therefore, the QD field is given below [30]:

$$E_{QD} = \frac{1}{\varepsilon_{eff_QD}}\left(E_{ext} + E^{ddi}_{NPVO_2,1} + E^{ddi}_{NPVO_2,1}\right) \tag{5}$$

where $\varepsilon_{eff_{QD}} = \frac{2\varepsilon_b + \varepsilon_s}{3\varepsilon_b}$, while $E^{ddi}_{NPVO_2,j} = \frac{1}{4\pi\varepsilon_b}\frac{S_a P_{NPVO_2,j}}{R_j^3}(j = 1,2)$ indicates the induced field produced by $NPVO_2$ which interacts with the QD. The polarization of each $NPVO_2$ is given by $P_{NPVO_2,j} = 4\pi\varepsilon_b a_j^3[\gamma_j(\omega)\bar{E}_{NPVO_2,j}e^{-i\omega t} + \gamma_j^*(\omega)\bar{E}_{NPVO_2,j}e^{i\omega t}]$ where γ_j is the dipole polarizability of $NPVO_2$ for each nanoparticle j. $E_{NPVO_2,j}$ is the total field of each $NPVO_2$ which in addition to the external field has two terms from the field caused by the QD polarization and the field caused by another $NPVO_2$ which are written as follows [30]:

$$\begin{aligned} E_{NPVO_2,1} &= E_{ext} + \frac{S_a P_{QD}}{4\pi\varepsilon_b\varepsilon_{eff_{QD}}R_1^3} + \frac{S_a P_{NPVO_2,2}}{4\pi\varepsilon_b\varepsilon_{eff_{NPVO_2},2}(R_1^3 + R_2^3)^3}, \\ E_{NPVO_2,2} &= E_{ext} + \frac{S_a P_{QD}}{4\pi\varepsilon_b\varepsilon_{eff_{QD}}R_2^3} + \frac{S_a P_{NPVO_2,1}}{4\pi\varepsilon_b\varepsilon_{eff_{NPVO_2},1}(R_1^3 + R_2^3)^3} \end{aligned} \tag{6}$$

Using the density matrix, QD polarization could be presented based on its off-diagonal elements as $P_{QD} = \mu(\rho_{12} + \rho_{21})$ where μ is the transition dipole moment, $\rho_{12} = \rho_{12}e^{-i\omega t}$ and $\rho_{21} = \rho_{21}e^{i\omega t}$ represent the density matrix elements that change with time, and $\varepsilon_{eff_{NPVO_2,j}} = \frac{2\varepsilon_b + \varepsilon_{NPVO_2,j}(\omega)}{3\varepsilon_b}(j = 1,2)$.

By performing mathematical calculations, the total field of the QD is obtained as follows [15,16]:

$$E_{QD} = \frac{\hbar}{\mu}\left[(\Omega + \eta\rho_{12})e^{-i\omega t} + (\Omega + \eta\rho_{21})e^{i\omega t}\right] \tag{7}$$

where Ω and η are respectively the Rabi frequency and the self-interaction of the QD which are given as follows:

$$\Omega = \frac{E_0 \mu}{2\hbar \varepsilon_{eff_{QD}}} \left\{ 1 + \frac{\frac{S_a a_1^3 \gamma_1}{R_1^3}\left(1 + \frac{S_a a_2^3 \gamma_2}{\varepsilon_{eff_{NPVO_2},2}(R_1+R_2)^3}\right)}{1 - \frac{S_a^2 a_1^3 \gamma_1 a_2^3 \gamma_2}{\varepsilon_{eff_{NPVO_2},1}\varepsilon_{eff_{NPVO_2},2}(R_1+R_2)^3}} + \frac{\frac{S_a a_2^3 \gamma_2}{R_2^3}\left(1 + \frac{S_a a_1^3 \gamma_1}{\varepsilon_{eff_{NPVO_2},1}(R_1+R_2)^3}\right)}{1 - \frac{S_a^2 a_1^3 \gamma_1 a_2^3 \gamma_2}{\varepsilon_{eff_{NPVO_2},1}\varepsilon_{eff_{NPVO_2},1}(R_1+R_2)^3}} \right\},$$

$$\eta = \frac{S_a^2 \mu^2}{4\pi \varepsilon_b \hbar \varepsilon_{eff_{QD}}^2} \left\{ \frac{\frac{a_1^3 \gamma_1}{R_1^3}\left(\frac{1}{R_1^3} + \frac{S_a a_2^3 \gamma_2}{\varepsilon_{eff_{NPVO_2},2} R_2^3 (R_1+R_2)^3}\right)}{1 - \frac{S_a^2 a_1^3 \gamma_1 a_2^3 \gamma_2}{\varepsilon_{eff_{NPVO_2},1}\varepsilon_{eff_{NPVO_2},2}(R_1+R_2)^3}} + \frac{\frac{a_2^3 \gamma_2}{R_2^3}\left(\frac{1}{R_2^3} + \frac{S_a a_1^3 \gamma_1}{\varepsilon_{eff_{NPVO_2},2} R_1^3 (R_1+R_2)^3}\right)}{1 - \frac{S_a^2 a_1^3 \gamma_1 a_2^3 \gamma_2}{\varepsilon_{eff_{NPVO_2},1}\varepsilon_{eff_{NPVO_2},2}(R_1+R_2)^3}} \right\} \quad (8)$$

The Hamiltonian of the QD with ground $|1\rangle$ and excited $|2\rangle$ states, whose energy difference is $\hbar\omega_0$, is expressed as follows [30]:

$$H_{QD} = \hbar\omega_0 \hat{a}^\dagger \hat{a} - \mu . E_{QD}(\hat{a} + \hat{a}^\dagger) \quad (9)$$

where $\hat{a}^\dagger$ is the ground state creation operator and $\hat{a}$ is the excited state annihilation operator.

By employing the density matrix technique and the equation of motion for the density matrix operator ($\frac{\partial \rho_{nm}(t)}{\partial t} = -\frac{i}{\hbar}\left[H_{QD}, \rho(t)\right]_{nm} + \Gamma(\rho),$) we present the density matrix elements to facilitate the investigation of energy transfer and QD behavior [31]:

$$\frac{d\Delta_\rho}{dt} = -2\Gamma_{21}\rho_{22} + 2i((\Omega + \eta\rho_{21})\rho_{12} - (\Omega + \eta\rho_{21})^* \rho_{21}) \quad (10)$$

$$\frac{d\rho_{21}}{dt} = -[i(\Delta_k - \eta_R \Delta_\rho) + (\gamma_{21} + \eta_I \Delta_\rho)]\rho_{21} + i\Omega\Delta_\rho \quad (11)$$

where $\Delta_\rho = \rho_{22} - \rho_{11}$ indicates the difference between the first two states in the QD and $\Delta_k = \omega_0 - \omega$ is the detuning frequency between the laser field and the excitonic transition. $\eta_I \Delta_\rho$ and $\eta_R \Delta_\rho$ respectively show the Förster broadening factor of the exciton transition and the energy shift of this transition in which $\eta_R = Real(\eta)$ and $\eta_I = Imag(\eta)$.

Moreover, in this structure, the absorption of the QD due to the transition $|2\rangle \leftrightarrow |1\rangle$ is calculated through the imaginary part of $Im(\rho_{21})$. To solve the dynamic equations (10) and (11), the fourth-order Rang-Kutta method is used.

3. DISCUSSION AND NUMERICAL RESULTS

In the present section, the effect of $NPVO_2$ in several phases on the optical properties of QD in the $NPVO_2$-QD-$NPVO_2$ plexitonic system is studied. The following parameters are employed in our calculations: $a = 4\,nm$ and $R_1 = R_2 = 20\,nm$. Γ_{12}=1.25ns^{-1} is the spontaneous radiative decay [26]. The dielectric constant of the environment is $\varepsilon_b = 2.25$. Using Mie theory, the absorption cross-section for the metallic phase of $NPVO_2$ at $\omega_{21} = 1.08\,eV$ ($\lambda = 1140\,nm$) has a resonant peak which indicates the excitation of SPPs. Given that the absorption peak in the metallic phase of $NPVO_2$ is in the infrared region, the QD Ag_2S, where the excitonic transition $|1\rangle \rightarrow |2\rangle$ is located ($\omega_{21} = 1.08\,eV$), is considered. Silver sulfide (Ag_2S) QD is assumed as a remarkable and appropriate choice for the present research. Silver sulfide was chosen because it has been experimentally proved to have very interesting absorption characteristics in the infrared (IR) region [28]. In particular, in this region, we note the excited transition $|2\rangle \leftrightarrow |1\rangle$, which corresponds to the characteristic resonance energy. This resonance energy is specifically detectable with the metallic phase of $NPVO_2$ caused by surface plasmon resonance.

Fig. 5 shows the imaginary part ρ_{21} which represents the absorption spectra of the QD for different phases (different fs where $f = 0$ stands for the semiconducting phase and $f = 1$ represents the metallic phase) versus Δ_k. In this figure, the radii of the NPs and QD are constant, with the filling fraction f changing only with temperature. The figure illustrates two $NPVO_2$, which alter both the energy shift and the absorption profile near the energy transition. As f increases, the absorption profile decreases and shifts further and the bandwidth of the absorption spectrum also expands. This behavior can be attributed to the interactions between the QD and the NPs which are strongly influenced by the local environment and the thermal dynamics of the nano-system. When temperature increases, the increased filling fraction f leads to enhanced electron-phonon coupling, which in turn modifies the optical characteristics of the hybrid system.

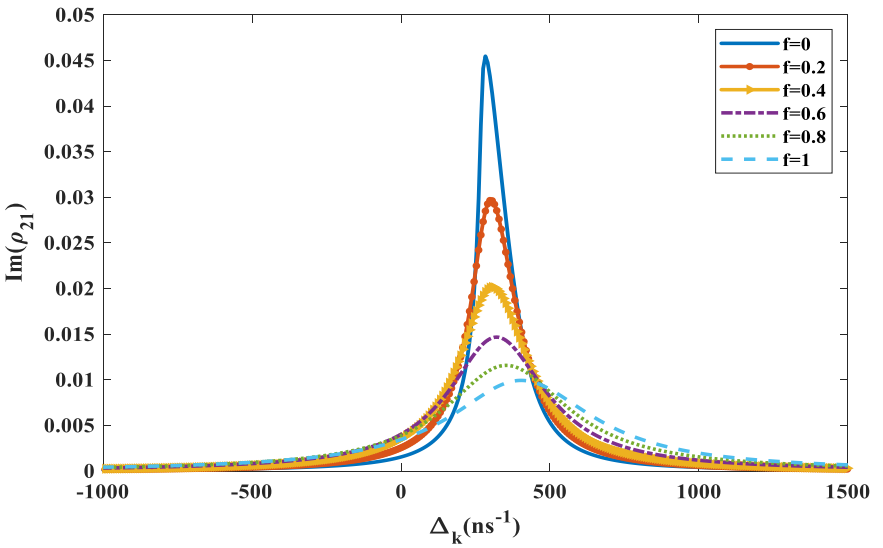

Fig. 5 The imaginary part of ρ_{21} indicating the absorption spectra of the QD versus Δ_k for different f s.

To investigate the impact of the NPs on the optical characteristics of the QD, Fig. 6 illustrates the imaginary part of ρ_{21} for three cases: (1) two $NPVO_2$ located on the two sides of the QD ($NPVO_2$-QD-$NPVO_2$); (2) a hybrid system with only one nanoparticle on one side of the QD ($NPVO_2$-QD); (3) a single QD. The results indicate that with the presence of two $NPVO_2$ in the semiconducting phase, the coupling is strong owing to the dipole/multipole interaction and that the absorption spectrum shows a blue shift due to the Rabi frequency which is in phase with the induced field.

In (2) or (3), a nanoparticle is located on one side of the quantum dot or the quantum dot is single considering that $Im(\rho_{21})$ represents the absorption of the system. These cases (2, 3) are in very good agreement with a previous work [26] which calculated the absorption of $NPVO_2$-QD hybrid system.

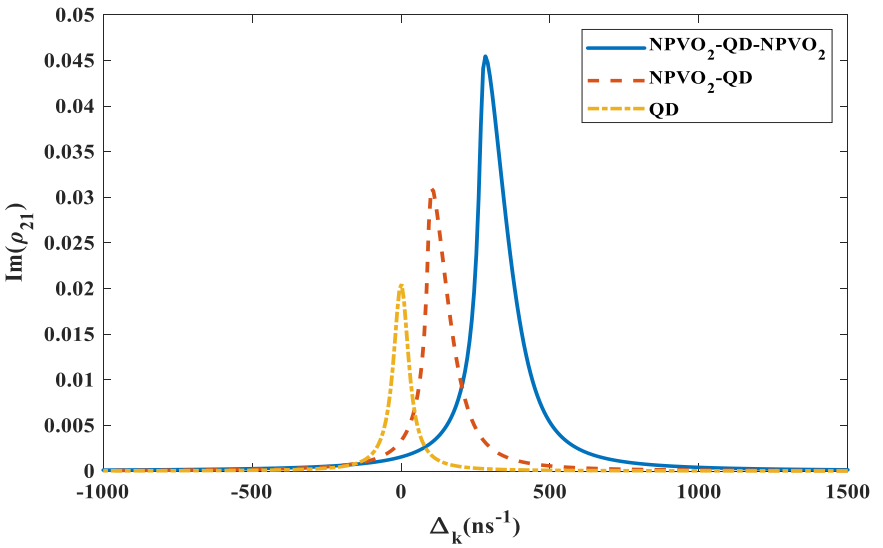

Fig. 6 The imaginary part of ρ_{21} versus the tunable exciton frequency and laser field energy for the three different states of the presence or absence of $NPVO_2$

Figure 7 illustrates how temperature changes affect field enhancement in the strong-field region. The results indicate a significant coupling in the semiconducting phase due to dipole/multipole interactions. The field is what the QD senses and it is shown that there is no field enhancement when $\Delta_k = 0$. In the semiconducting phase, the field enhancement is about 5.5 times in the transition energy difference of $285\, ns^{-1}$. As f increases, the field enhancement peak diminishes and energy shifts further.

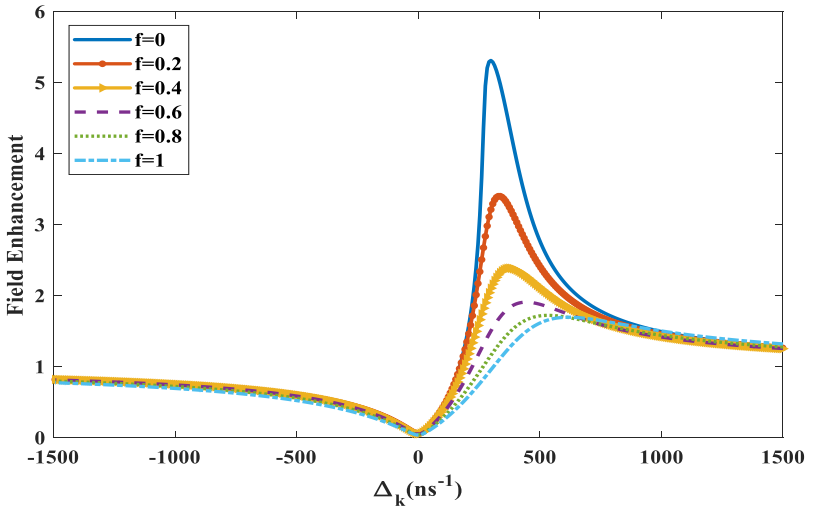

Fig. 7 The field enhancement of the $NPVO_2$-QD-$NPVO_2$ hybrid system based on the transition energy difference

To investigate the behavior of $\eta_R\Delta_\rho$ when the $NPVO_2$-QD-$NPVO_2$ hybrid system is considered, it is plotted in Fig. 8 for different phases versus a frequency close to the transition frequency.

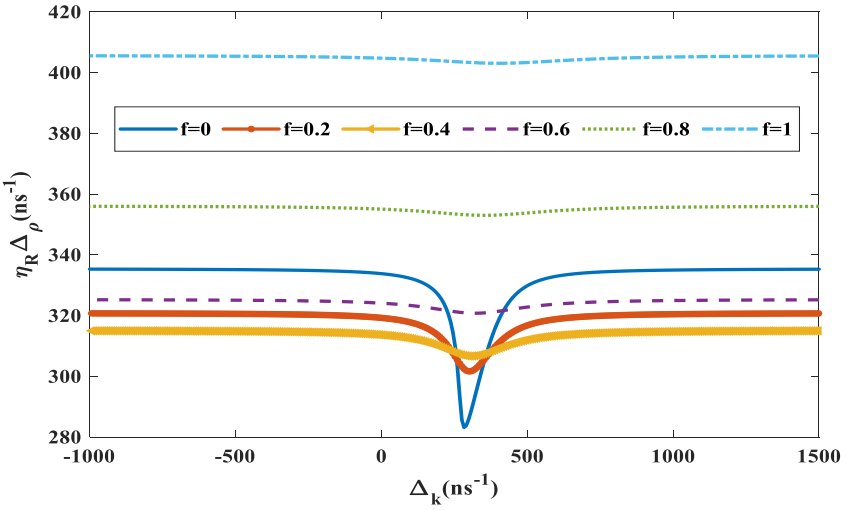

Fig. 8 The energy shift of the exciton transition ($\eta_R\Delta_\rho$) versus Δ_k

The figure shows that as f increases, the exciton transition energy shift also increases, resulting in a blue shift. At $f=0$, near the $|1\rangle \leftrightarrow |2\rangle$ transition ($\Delta_k = 285\, ns^{-1}$), the lowest exciton transition energy shift occurs. In contrast, when f=1 and frequencies are away from the $|1\rangle \leftrightarrow |2\rangle$ resonance, the exciton transition energy shift reaches approximately 405 ns^{-1}.

The effect of phase change as an effective parameter can be shown in the broadening of the Förster energy. This process is normalized by the exciton population in the presence of quantum coherence. Therefore, Fig. 9 shows the parameter $\eta_I \Delta_\rho$ for the strong-field regime. The effect of this parameter is expressed in Eq. (12). As f increases, the Förster-enhanced broadening factor due to dipole/multipole also rises, changing from 41 ns^{-1} to 275 ns^{-1} as f shifts from 0 to 1, even at frequencies away from resonance.

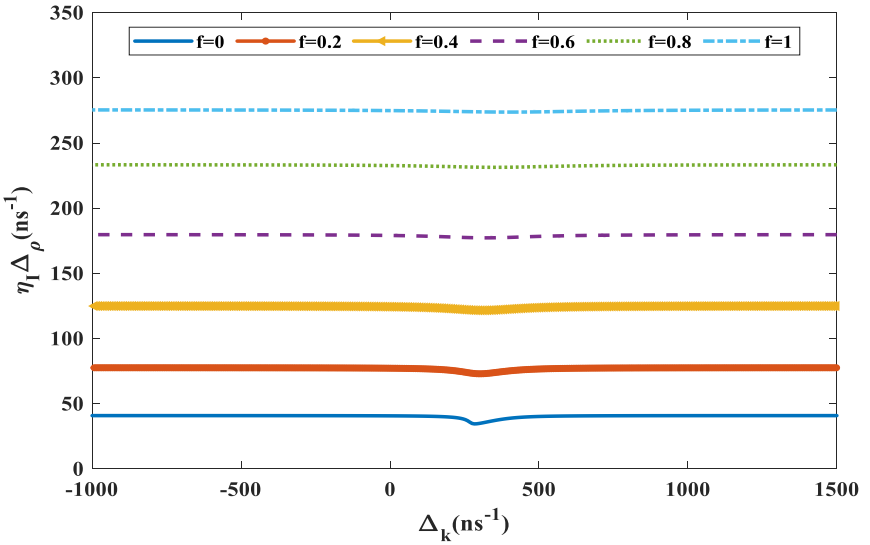

Fig. 9 Förster-enhanced broadening factor ($\eta_I \Delta_\rho$) according to the tunability of the exciton energy transition and the laser field ($\Delta_k = 0$)

4. CONCLUSION

To enhance the optical characteristics of QDs, one can incorporate NPs into them. In this approach, the interaction between excitons and plasmons changes the optical characteristics of the QD. In the present study, $NPVO_2$ NPs were employed. A notable finding was that with $NPVO_2$ present on both faces of the

QD in the strong-field region, the absorption spectrum altered, resulting in an absorption peak and a change in the resonance frequency of the QD. Furthermore, f significantly influenced the increase of the plasmonic field, exciton energy transition, and broadening. However, all these parameters were nearly zero at the transition frequency. For $NPVO_2$ NPs, the field increased approximately five-fold at 285 ns^{-1}, indicating the excitation of plasmons in this region.

However, this study demonstrated how varying the temperature of $NPVO_2$ affects the optical characteristics of the plexitonic system while its physical parameters remain unchanged.

REFERENCE

[1] R. Vincent, H. Marinchio, J. J. Sáenz, and R. Carminati. *Local control of the excitation of surface plasmon polaritons by near-field magneto-optical Kerr effect*. Physical Review B. 90(24) (Dec. 2014) 241412. Available: https://doi.org/10.1103/PhysRevB.90.241412.

[2] H. M. Ali, S. Abd-Elnabi, and K. Osman. *The intensity of the plasmon–exciton of three spherical metal nanoparticles on the semiconductor quantum dot having three external fields*. Plasmonics. 17(4) (Aug. 2022) 1633-1644. Available: https://doi.org/10.1007/s11468-022-01649-0.

[3] S. Z. Hosseini Minabi, A. Keshavarz, A. Gharaati, *The effect of temperature on optical absorption cross section of bimetallic core-shell nano particles*, JOPN, 1(3) (Aug. 2016) 67-76. Available: http://jopn.marvdasht.iau.ir/article_2203.html.

[4] Kh. Hemmati Kahradeh, E. Saievar Iranizad, A. Bayat, *Investigation of hydrothermal process time on the size of carbon micro- and nano-spheres*, JOPN, 2(2) (March 2019) 52-60. Available: http://jopn.marvdasht.iau.ir/article_2424.html.

[5] M. Servatkhah, P. Hashemi, R. Pourmand, *Binding energy in tuned quantum dots under an external magnetic field*, JOPN. 7(4) (Nov. 2022) 49. Available: https://doi.org/10.30495/jopn.2022.30924.1270.

[6] M. C. Larciprete, D. Ceneda, D. Scirè, M. Mosca, D. Persano Adorno, and M. Centini. *Tunable IR perfect absorbers enabled by tungsten doped VO2 thin films*. APL Materials. 11(9) (Sep. 2023) 091107. Available: https://doi.org/10.1063/5.0164410.

[7] M. J. Karimi, M. Soliemiani, H. Rahimi, *Light absorption and short-circuit current density in plasmonic organic solar cells containing liquid crystal and metal nanowires*. JOPN. 9(4) (Dec. 2024) 33625. Available: https://doi.org/10.30495/jopn.2024.33665.1325.

[8] H. Fouladi; A. Farmani; A. Mir, *Rigorous Investigation of Ring Resonator Nanostructure for Biosensors applications in breast cancer detection*, JOPN. 8(4) (Nov. 2023) 97. Available: https://doi.org/10.30495/jopn.2024.32304.1299

[9] L. Tan, X. Lu, L. Tang, K. Chen, J. Wang, and W. Huang. *Flexible composite film utilizing VO 2 self-adaptive photothermal and infrared radiative cooling for continuous energy harvesting*. Optics Express. 32(13) (Jun. 2024), 22675-22686. Available: https://doi: 10.1364/OE.523853.

[10] A. Bile, D. Ceneda, V. E. Maryam, D. Scirè, and M. C. Larciprete. *Room-temperature tuning of mid-infrared optical phonons and plasmons in W-doped VO2 thin films*. Optical materials. 154 (Aug. 2024) 115732. Available: https://doi.org/10.1016/j.optmat.2024.115732.

[11] M. A. Moghaddam, and N. Daneshfar. *Two-and three-photon absorption cross-section investigation in nanometer-sized heterodimer and heterotrimer structures*. The European Physical Journal Plus. 139(7) (Jul. 2024) 607. Available: https://doi.org/10.1140/epjp/s13360-024-05411-9.

[12] E. Paspalakis, S. Evangelou, and A. F. Terzis. *Control of excitonic population inversion in a coupled semiconductor quantum dot–metal nanoparticle system*. Physical Review B. 87(23) (Jun. 2013) 235302. Available: https://doi.org/10.1103/PhysRevB.87.235302.

[13] R. D. Artuso, and G. W. Bryant. *Optical response of strongly coupled quantum dot− metal nanoparticle systems: double peaked fano structure and bistability*. Nano letters. 8(7) (Iul. 2008) 2106-2111. Available: https://doi.org/10.1021/nl800921z.

[14] Y. Fedutik, V.V. Temnov, O. Schöps, U. Woggon, and M.V Artemyev. *Exciton-plasmon-photon conversion in plasmonic nanostructures*. Physical review letters. 99(13) (Sep. 2007) 136802. Available: https://doi.org/10.1103/PhysRevLett.99.136802.

[15] N. Daneshfar, and M. Mohammadbeigi. *Theoretical study of the nonlinear optical effects in tunable plasmon–exciton hybrid nanosystems: third-and fifth-order optical processes*. The European Physical Journal Plus. 138(5) (May 2023) 404. Available: https://doi.org/10.1140/epjp/s13360-023-04020-2.

[16] J. Yi, X. Han, X. Chen, C. Liu, and Y. Luo. *The enhanced two-photonexcited fluorescence of CdSe quantum dots on the surface of au island films from surface Plasmon resonance*. Thin Solid Films. 521 (Oct. 2012) 112-114. Available: https://doi.org/10.1016/j.tsf.2012.02.041.

[17] S. G. Kosionis, E. Paspalakis. *Tunneling induced transparency and slow light in an asymmetric double quantum dot molecule—Metal nanoparticle*

hybrid. Journal of Applied Physics. 134(24) (Dec. 2023) 243107. Available: https://doi.org/10.1063/5.0174151.

[18] . V. Bragas. *A nonlinear switching mechanism in quantum dot and metallic nanoparticle hybrid systems*. *Advanced Optical Materials*. 1(6) (Jun. 2013) 460-467. Available: https://doi.org/10.1002/adom.201300105.

[19] A. Hatef, S. M. Sadeghi, S. Fortin-Deschênes, E. Boulais, and M. Meunier. *Coherently-enabled environmental control of optics and energy transfer pathways of hybrid quantum dot-metallic nanoparticle systems*. Optics express. 21(5) (Mar. 2013) 5643-5653. Available: https://doi.org/10.1364/OE.21.005643.

[20] H. Mertens, J. S. Biteen, H. A. Atwater, and A. Polman. *Polarization-selective plasmon-enhanced silicon quantum-dot luminescence*. Nano letters. 6(11) (Nov. 2006) 2622-2625. Available: https://doi.org/10.1021/nl061494m.

[21] T. Pons, I. L. Medintz, K. E. Sapsford, S. Higashiya, A. F. Grimes, D. S. English, and H. Mattoussi. *On the quenching of semiconductor quantum dot photoluminescence by proximal gold nanoparticles*. Nano letters. 7(10) (Oct. 2007) 3157-3164. Available: https://doi.org/10.1021/nl071729+.

[22] P. Vasa, R. Pomraenke, S. Schwieger, Y. I. Mazur, V. Kunets, and G. Salamo. *Coherent exciton–surface-plasmon-polariton interaction in hybrid metal-semiconductor nanostructures*. Physical review letters. 101(11) (Sep. 2008)116801. Available: https://doi.org/10.1103/PhysRevLett.101.116801.

[23] S. Rashidi, S. R. Entezar. And A. Rashidi. *Kerr-nonlinearity-assisted NIR nonreciprocal absorption in a VO_2-based core–shell composite integrated with 1D nonlinear multilayers*. Applied Optics. 60(28) (Oct. 2021) 8651-8658. Available: https://doi: 10.1364/AO.438938.

[24] A. Rashidi. *Study of temperature distribution in a metallic nanograting based on a Kerr nonlinear material irradiated by a nanosecond pulsed laser*. Iranian Journal of Physics Research. 23(4) (Feb. 2024) 621-628. Available: https://doi.org/10.47176/ijpr.23.4.11778.

[25] S. A. Imam, K. M. Ishtiak and Q. D. Khosru. *Modelling a near perfect temperature tunable multiband VO2 based photonic-plasmonic absorber within visible and near infrared spectra*. Results in Engineering. 18 (Jun. 2023)101084. Available: https://doi.org/10.1016/j.rineng.2023.101084.

[26] A. Hatef, N. Zamani, W. Johnston. *Coherent control of optical absorption and the energy transfer pathway of an infrared quantum dot hybridized with a VO_2 nanoparticle*. Journal of Physics: Condensed Matter. 29(15) (Mar. 2017) 155305. Available: https://doi.org/10.1088/1361-648X/aa61ee.

[27] U. K. Chettiar, and N. Engheta. *Modeling vanadium dioxide phase transition due to continuous-wave optical signals*. Optics Express. 23(1) (Jan. 2015) 445-451. Available: https://doi.org/10.1364/OE.23.000445.

[28] T. Kikuzuki, and M. Lippmaa. *Characterizing a strain-driven phase transition in VO_2*. Applied Physics Letters. 96(13) (Mar. 2010) 132107. Available: https://doi.org/10.1063/1.3380599.

[29] H. T. Kim, Y. W. Lee, B. J. Kim, B. G. Chae, S. J. Yun, S. J., and Y. Lim. *Monoclinic and correlated metal phase in VO2 as evidence of the Mott transition: coherent phonon analysis*. Physical review letters. 97(26) (Dec. 2006) 266401. Available: https://doi.org/10.1103/PhysRevLett.97.266401.

[30] N. Zamani, H. Nadgaran, and A. Hatef. *The effect of quantum correction for the dielectric function on the optical properties of a plasmon–exciton–plasmon hybrid system*. *The European Physical Journal D*. 75 (Jan 2021) 1-7. Available: https://doi.org/10.1140/epjd/s10053-021-00053-3.

[31] M. C. Ko, N. C. Kim, C. J. Jang, G. J. Kim, Z. H. Hao and Q. Q Wang. *Control of the Optical Response of an Artificial Hybrid Nanosystem Due to the Plasmon-Exciton Plasmon Coupling Effect*. arXiv preprint arXiv:1708. (Aug. 2017) 06636 Available: https://doi.org/10.48550/arXiv.1708.06636.